Hydrophilic properties of soot particles exposed to OH radicals: A possible new mechanism involved in the contrail formation

Symphorien Grimonprez, Junteng Wu, Alessandro Faccinetto, Sylvie Gosselin, Eleonore Riber, Bénédicte Cuenot, Mathieu Cazaunau, Edouard Pangui, Paola Formenti, Jean-François Doussin, et al.

Hydrophilic properties of soot particles exposed to OH radical: a possible new mechanism involved in the contrail formation

Symphorien Grimonprez[1], Junteng Wu[1], Alessandro Faccinetto[1], Sylvie Gosselin[1], Eleonore Riber[2], Bénédicte Cuenot[2], Mathieu Cazaunau[3], Edouard Pangui[3], Paola Formenti[3], Jean-François Doussin[3], Denis Petitprez[1], Pascale Desgroux[1*]

[1] *Univ. Lille, CNRS, UMR 8522 - PC2A - Physicochimie des Processus de Combustion et de l'Atmosphère, F-59000 Lille, France*

[2] *CERFACS, 42 Av. G. Coriolis Toulouse cedex, France*

[3] *Laboratoire Interuniversitaire des Systèmes Atmosphériques (LISA), UMR7583, CNRS, Université Paris-Est-Créteil (UPEC) et Université de Paris, Institut Pierre Simon Laplace (IPSL), Créteil, France*

Abstract

This work investigates the role of soot particles in the early steps of formation of condensation trails (contrails). Contrails are thin linear clouds that form behind cruising aircrafts and can evolve into persistent clouds, and therefore can contribute to the radiative forcing of the atmosphere. Mitigating their contribution is considered an efficient way for decreasing the radiative forcing. Condensation freezing is proposed as a major pathway leading to the heterogeneous nucleation of ice particles in the aircraft exhausts. Soot particles, freshly produced in the flames and not significantly oxidized in the post-flame, are hydrophobic. Therefore, many theoretical and experimental approaches that investigate contrails formation introduce prior activation by surface adsorption of sulfur compounds issued from kerosene combustion. Even though the role of sulfur content of the fuel is unclear, and may only weakly impacts contrails formation, many simulations still rely on this assumption. In this work, to elucidate the role of sulfur compounds on the activation of soot chemically aged with OH radicals, a comparative study is performed with soot sampled from a turbulent jet flame burning a sulfur-containing fuel (kerosene) and a sulfur-free fuel (diesel). Soot aging experiments are performed in the atmospheric simulation chamber CESAM, with controlled generation of OH radicals. Soot activation (ratio between the number of nucleated droplets and seeding particles) is measured in water supersaturation conditions. OH exposure significantly enhances soot activation regardless of the sulfur presence in the fuel. The possibility for soot oxidation by OH radicals formed in aeronautical engines to be sufficient to promote soot activation is explored. Large eddy simulation in the high pressure turbine is used to model the fluid particle and OH trajectories and their chemical evolution. Residence time in the turbine is found sufficient to activate soot particles, opening a new possible route to explain ice particles formation.

Keywords: Soot, OH oxidation, aeronautical engine, κ-Köhler theory, contrail

1. Introduction

Condensation trails (contrails) are thin linear clouds that form behind cruising aircrafts and can evolve into persistent clouds. A change in global cloud coverage due to aircraft induced clouds (AIC) results in a radiative forcing of the atmosphere. The contribution of AIC accounts for more than 50 % of forcing fraction within aviation components, larger than CO_2 (40%) [1]. Thus, mitigating the contribution of AIC is an efficient and prompt way for decreasing radiative forcing since it can be operated at much shorter time scale than the reduction of aircraft CO_2 emissions. Properties of individual contrails are highly documented [2]. However, the formation process of freshly formed contrails is not fully understood.

The Schmidt-Appleman criterion [3], often used to determine whether a contrail can form, requires that supersaturation conditions with respect to ice or liquid water be fulfilled locally in the plume of the aircraft exhausts mixing with cold ambient air. A maximum threshold temperature involving the water emission index, the fuel combustion heat and the propulsion efficiency of the aircraft at cruise [4] can be determined. Condensation freezing has been proposed as a major pathway leading to the heterogeneous nucleation of ice particles in the aircraft exhausts. The number of ice particles is closely related to the soot emission index [4]. Several approaches also introduce a priori activation of soot particles to make them hydrophilic, activation representing the particle propensity to form liquid droplets or ice nuclei. For instance, the activation process has been modeled by considering the adsorption of sulfur compounds in exhaust of kerosene combustion on the surface of soot particles [5]. Activated particles then form liquid water droplets by scavenging ultrafine water droplets already existing in the gas plume, and subsequently freeze through contact or immersion freezing [6]. There is no clear consensus in the literature about the role of sulfur in the formation of contrails [1-8]. However the recent review of the properties of contrails [2] reports that the changes in fuel sulfur content (FSC) were found to have minimal impact on contrail onset. Even though the content of sulfur in the fuel has probably a weak impact on the formation of contrails [2], many simulations still rely on this assumption [6–8].

The importance of soot particles as cloud condensation nuclei (CCN) has led to several experimental investigations at ambient pressure and temperature. Freshly emitted soot particles, either from engines [9] or laboratory flames [10], are hydrophobic and are therefore considered as poor CCN. However, their activity increases after being exposed to ozone [10,11], OH radicals [10,12] or sulfur oxides [13]. It was also shown that soot maturity [11] and soot particle size [10] significantly affect soot activation under oxidative exposure.

In this work, to elucidate the role of sulfur compounds on the activation of aeronautic soot, a comparative laboratory study is performed for the first time with soot sampled from a turbulent jet flame burning a sulfur-containing fuel (kerosene) and a sulfur-free fuel (diesel). In order to activate the soot particles, they are aged in the CESAM simulation chamber (French acronym for experimental multiphasic atmospheric simulation chamber) [14], with controlled concentrations of OH radicals. Indeed the possibility that OH is an effective agent activating aeronautic soot particles is evocated in [15]. For different OH exposures, soot activation is measured in water supersaturation conditions using a commercial cloud condensation nuclei counter (CCNc). According to κ-Köhler theory [16], the hygroscopicity parameter κ is calculated following a theoretical approach that we recently proposed [17]. In the final section of this work, the experimental results are used to determine if the soot aging in the turbine of an aeronautical engine would be sufficient to activate the emitted soot particles. For that purpose, OH concentration is calculated based on the results of a previous Computational Fluid Dynamics (CFD) simulation of the turbine.

2. Experimental set-up and procedures.

Figure 1 shows a scheme of the experimental setup. Soot particles are produced in a turbulent diffusion flame supplied with kerosene or diesel fuel. Particles are sampled on the flame axis at 130 mm height above the burner (HAB) with a diluting quartz microprobe specifically developed for

scanning mobility particle size (SMPS) measurements. This system allows fast dilution of the sampled gas [11].

The sampled flow passes through a diffusion denuder (activated charcoal parallel plates). Then, soot particles are injected in the CESAM chamber in which they are aged under oxidation by OH radicals. After aging, soot particles are size-selected at a well-defined electrical mobility with a differential mobility analyzer (DMA), then the flow is split between the CCNc and a condensation particle counter (CPC) as shown in Figure 1. The number of generated water droplets is counted by the CCNc and the number of soot particles by the CPC. Their ratio determines the activated fraction for each water supersaturation [11].

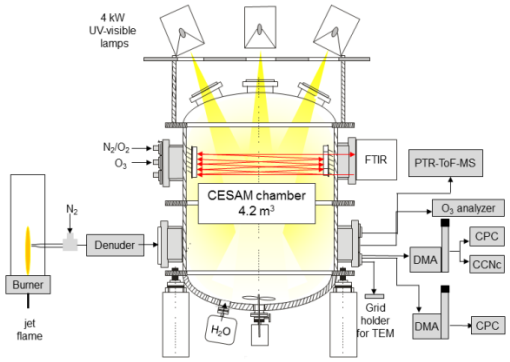

Figure 1: Schematic of the experimental setup

2.1 Generation of soot particles

Two fuels have been tested: kerosene Jet A1 (sulfur content 700 ppm [18]) and ultra-low sulfur diesel (<10 ppm). The chemical composition of the fuels is analyzed by gas chromatography/mass spectrometry (GC/MS). The main composition of the fuels is provided in Supplemental Material 1 (SM1).

Turbulent jet flames are stabilized on an atmospheric hybrid Holthuis burner composed of a 60-mm bronze porous plug with a central tube allowing the introduction of a DIHEN (model 170AA) nebulizer [19]. The flow rate of the nebulization gas (nitrogen) is fixed to 0.22 L min^{-1}. Kerosene and diesel are introduced in the nebulizer capillary with a mass flow rate of 50 g h^{-1} controlled with a liquid mass

flow controller (Bronkhorst High-Tech L2C2I). A high speed spray of small liquid fuel droplets is formed at the exit of the nebulizer and is ignited by a lean premixed methane–air flat flame (equivalence ratio = 0.8, cold velocity 13 cm/s) stabilized on the porous. The resulting turbulent sooting diffusion flames are stabilized with very similar characteristics in terms of shape, height, width and sooting patterns for a large range of liquid fuels [19]. Particularly, the soot volume fraction of the flames peaks at the same HAB (130 mm with the present nebulizer) and it is found 25 % higher in the diesel flame than in the kerosene flame [19].

At their peak location, soot particles are mature and have experienced very weak oxidation. They have close primary particle diameter according to previous time-resolved laser induced incandescence investigations [19]. This is confirmed by transmission electron microscopy (TEM) investigations of kerosene [11] and diesel [20] soot, which lead to a mean diameter of the primary particles of 16.7 nm and 16.3 nm respectively.

The chemical composition of soot particles issued from diesel and kerosene combustion is determined by GC-MS (Clarus 600/680 PerkinElmer) after dichloromethane extraction. The analysis of the extracts reveals very similar concentration of polycyclic aromatic composition from naphthalene to coronene (SM2). A few oxygenated compounds are also found in kerosene soot. However, the sensitivity of GC/MS is insufficient to identify sulfur compounds in the soot bulk as recently observed by comparison with X-ray photoemission spectroscopy [18].

Sulfur compounds such as SO_2 are present in the burnt gases of flames fueled with sulfur-containing fuels as kerosene [21]. In this work, a denuder is inserted between the sampling probe and the simulation chamber in order to prevent secondary organic aerosol (SOA) formation in the chamber. SO_2 traces in the CESAM chamber were not detected using in-situ multipath cell (182.50 m) Fourier transform infrared spectroscopy (Bruker® Tensor37™, detection limit of 50 ppbV).

To summarize, soot particles sampled at 130 mm in the two investigated flames have close morphology and chemical composition, except for the presence of some oxygenated compounds in kerosene soot not detected on diesel soot.

2.2 **Generation of cloud condensation nuclei**

The CCN activity of soot particles is investigated against water supersaturation SS_w [9,10,22] by means of a commercial continuous-flow thermal-gradient cloud condensation nuclei counter CCNc-100, Droplet Measurement Technologies. SS_w is generated in the instrument using a vertical thermal gradient and continuous humidification through the inner column. By changing the temperature gradient, SS_w = 0.07-1.8% can be obtained. The calibration of the instrument is performed according to the procedure detailed in [11]. The number of nucleated water droplets and the particle concentration in the CESAM chamber, required to calculate the activated fraction F_a, are measured in parallel by a CCNc (sampling flow 0.5 $Lmin^{-1}$) and a TSI CPC3776 (sampling flow 0.3 $Lmin^{-1}$) downstream the DMA TSI 3081 (sheath/sample flow ratio set to 10). During the aging experiments, the initial d_m is selected as 150 nm by a DMA upfront the CCNc and CPC analyzers.

2.3 CESAM chamber

Experiments are performed in the CESAM chamber described in detail elsewhere [14]. The facility consists of 4.2 m^3 stainless steel cylindrical vessel. Above the chamber, three high-pressure xenon arc lamps (4 kW, MH Diffusion®, MacBeam™ 4000) equipped with 6.5 mm thick Pyrex filters provide irradiation with a spectrum very similar to the solar spectrum [14]. Temperature and relative humidity were measured using a Vaisala® probe (HMP234).

Experiments begin by filling the chamber with clean dry air to 10 mbar above the atmospheric pressure p_a by mixing approximately 800 mbar of nitrogen produced from the evaporation of a pressurized liquid nitrogen tank (Messer, purity > 99.995 %) and 200 mbar of oxygen (Linde gaz ,

oxygen purity 99.999 %). To enable the introduction of soot particles sampled from the flame, the initial pressure of the chamber is decreased down to 20 mbar below p_a, and after injection adjusted with synthetic air up to 10 mbar above p_a. The temperature of the chamber is set to 293±1 K.

Sampling flow to instrumental sampling from the chamber is continuously compensated by a flow of dry synthetic air adjusted to keep the overall pressure constant. This compensation flow is continuously recorded by the CESAM control system and the values are used to evaluate the dilution rates in the chamber prior to the calculation of any chemical rates.

The controlled OH generation in CESAM relies on the photolysis of ozone forming oxygen atom (O^{1D}), $O_3 + h\nu \rightarrow O^{1D} + O_2$ (whose photolysis frequency is hereafter noted J_{O1D}) followed by reaction with water forming OH radicals $O^{1D} + H_2O \rightarrow 2\ OH$.

To set the relative humidity to the required value (20%), water vapor is pressurized in a 5 L stainless steel vessel filled with ultrapure water (Elga 18.2 MΩ.cm). Using this setup, starting from dry conditions in the chamber (<1% RH), 20% RH is reached in less than 5 minutes.

An ozone generator (BMT 802N) is used to introduce 1 ppm ozone in CESAM. OH exposure starts when the lights are switched on. 40 ppb of 3-pentanol (Sigma-Aldrich, 98%), used as OH tracer, is injected in the chamber [23]. 3-pentanol is followed on-line thanks to a proton transfer reaction time-of-flight mass spectrometry (Kore Technology ltd, PTR-TOF-MS, Series II). The concentration of 3-pentanol is derived from the 71 *m*/z ion that is typical from its reaction with H_3O^+ [$M+H^+-H_2O$]). The rate constant used to calculate OH concentrations is $k_{3\text{-pentanol+OH}}(298.15\ K)=(1.11 \pm 0.1) \times 10^{-11}$ cm^3 $molecule^{-1}s^{-1}$ [24]. For some experiments, to increase the photolysis of O_3 and the OH production, the Pyrex filters of the irradiation system are removed leading to $J_{O1D}= (1.50 \pm 0.1)\times10^{-4}$ s^{-1} with Pyrex filters and $J_{O1D}= (1.51 \pm 0.1)\times10^{-3}$ s^{-1} without filters. Detailed experimental conditions are reported in SM3.

3. Determination of the hygroscopic parameter

In order to determine the hygroscopicity parameter κ, an extension of κ-Köhler theory [16] that takes into account the effect of the dry particle size distribution [25], the complex morphology of soot [17] and a distribution of κ values [26] is used. This model [16] is applied here to fit the activation curves (§4.2.1). The modeled F_a is described as:

$$F_a(SS) = \sum_{\kappa=0}^{\infty} \left\{ \frac{1}{2} - \frac{1}{2} \operatorname{erf} \left[\frac{\ln d_p(\kappa, SS) - \ln \mu_{p,geo}}{\sqrt{2} \ln \sigma_{p,geo}} \right] \right\} p(\kappa) \Delta\kappa \qquad \text{Equation 1}$$

where d_p is the diameter of the dry particle assumed to be spherical, $\mu_{p,geo}$ and $\sigma_{p,geo}$ are the geometric mean and standard deviation of d_p, respectively. p(κ) is the probability density function of κ:

$$p(\kappa) = \frac{1}{\kappa \ln \sigma_{\kappa,geo} \sqrt{2\pi}} e^{-\frac{[\ln \kappa - \ln \mu_{\kappa,geo}]^2}{2 \ln^2 \sigma_{\kappa,geo}}} \qquad \text{Equation 2}$$

where $\mu_{\kappa,geo}$ and $\sigma_{\kappa,geo}$ are the geometric mean and standard deviation of κ, respectively.

Being soot particles fractal-like objects, it is necessary to consider an equivalent diameter in alternative to d_p. A morphology-corrected volume equivalent diameter d_{ve} can be calculated [17,27] from the electrical mobility d_m, the diameter of primary particles d_{pp}, the number of primary particles per aggregate N_{pp} and the aggregate fractal dimension D_f (see Table 1), following the conversion model proposed by Yon et al. [27].

Table 1: Morphological parameters of soot particles selected and sent to the CCNc with d_m = 150±1 nm: primary particle diameter (d_{pp}, nm), fractal dimension D_f, geometric mean $\mu_{p,geo}$ and standard deviation $\sigma_{p,geo}$ of d_m distribution (nm), volume equivalent diameter d_{ve} (nm). d_{pp} and D_f are determined from TEM analysis [11,20]. The uncertainty on d_{pp} and $\mu_{p,geo}$ is ± 0.9 nm and on d_{ve} is ±0.5 nm.

Fuel	d_{pp}	D_f	$\sigma_{p,geo}$	$\mu_{p,geo}$	d_{ve}
kerosene	16.7	1.65	1.06	150.5	93.5
diesel	16.3	1.8	1.06	150.5	107.5

The only two free parameters of the fitting are the geometric mean and standard deviation of the κ distribution $\mu_{\kappa,\mathrm{geo}}$ and $\sigma_{\kappa,\mathrm{geo}}$.

4. Experimental results.

The main objective of the study is to compare the CCN activity of kerosene and diesel soot particles exposed to OH. We sampled intentionally mature (i.e. weakly reactive [11]) soot particles at HAB=130 mm, having experienced only weak oxidation, in order to have afterwards a perfect control on the oxidation impact in the simulation chamber.

4.1 Evolution of the particle size distribution over time.

To achieve a large range of OH exposure ([OH] × residence time), soot particles are exposed to OH during various periods in CESAM. During this period, the soot size distribution is affected by coagulation processes due to the large initial particle concentration. The evolution of the soot size distribution, continuously monitored using a SMPS TSI 3080 over a period of 6 h (3 min time resolution) is presented in Fig.2. The initial total concentration of soot particles sampled in the kerosene flame and introduced in the chamber is 10.3×10^4 cm^{-3}. During the aging period, d_m increased from 103±1 nm to 178±1 nm. Although this increase is significant, it is not expected to affect the interpretation of the results since the particles are size selected around their peak at d_m = 150 nm regardless of their residence time in CESAM. Furthermore, the normalized size distributions are not affected by the presence of OH. Similar results are found for diesel soot (SM4).

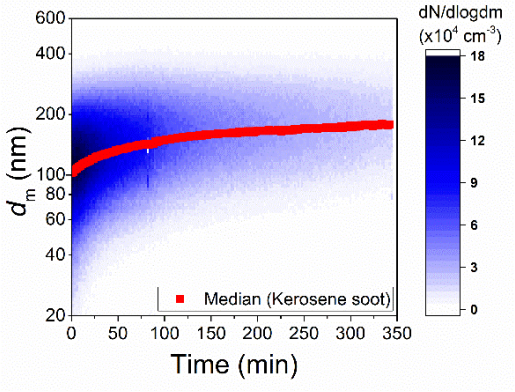

Figure 2: d_m of kerosene soot versus aging time in CESAM. Concentration is represented by white-blue heat map. Solid red squares represent the median of the size distribution. t=0 refers to the OH generation.

It is worth noting that the flow rates have not been optimized to prevent aggregation and coagulation in the sampling line but rather to assure the correct operation of the measurement instruments. Thus, the collected size distributions are representative of the sampling line and not of the flame.

4.2 Soot as CCN

The OH concentration is varied between 10^5 to 10^7 molecule cm^{-3}. The exposure time is varied between 70 and 340 min resulting in a large range of exposures: [1.6-19]× 10^{10} molecule cm^{-3} s.

4.2.1 Activation curves for kerosene soot and κ determination

This section only describes experiments performed on kerosene soot particles. The same measurements performed on diesel soot particles are shown in SM4.

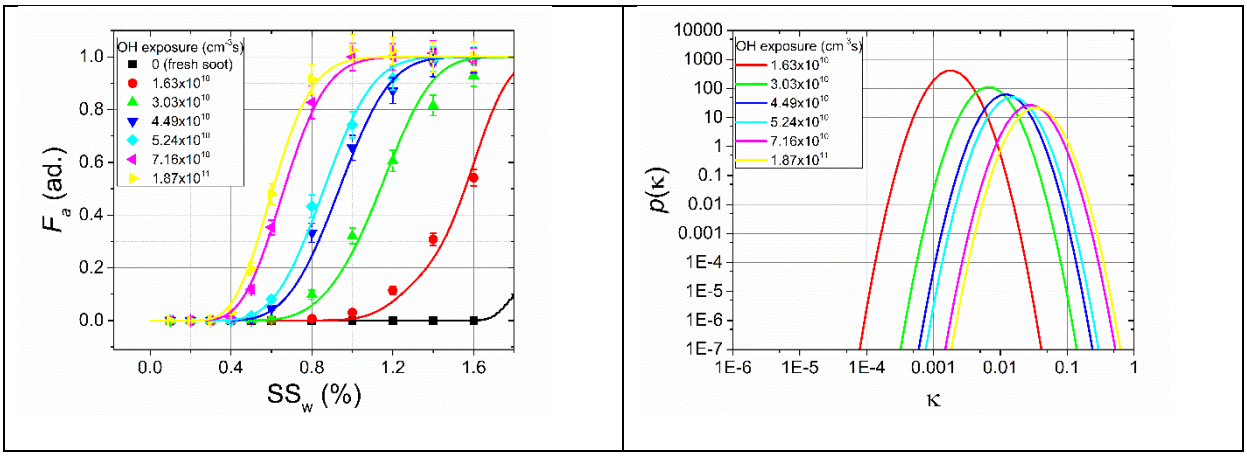

Figure 3: (a) Activated fraction F_a versus water supersaturation SS_w: activation curves of kerosene soot particles exposed to OH radicals. Experimental data (solid points) are fitted using the extended κ-Köhler model [17]. (b) probability density function p(κ) versus hygroscopicity parameter κ: log normal distribution of κ of kerosene soot particles exposed to OH radical.

Fig. 3a shows F_a against SS_w for the range of investigated OH exposures. From the activation curves, one can determine the critical supersaturation SS_c, corresponding to the value of supersaturation for which F_a = 0.5, which is the minimum SS_w above which an ideal spherical droplet can grow indefinitely. Our results show that SS_c decreases with increasing OH exposure, indicating that aged soot particles are activated at progressively lower SS_w. This could result from heterogeneous reactions between OH radicals and the surface of soot forming oxygenated polar species, henceforth enhancing the soot affinity with water vapor [10]. It is noteworthy that natural oxidation within the flame is insufficient to activate fresh soot particles since they are found inactive at SS_w as high as 1.6%, consistently with the literature [9,10].

Fig. 3b shows p(κ) of kerosene soot measured at different OH exposure. According to the model sensitivity study [17], $\mu_{\kappa,\text{geo}}$ is set as a free parameter while $\sigma_{\kappa,\text{geo}}$= 1.6 is kept fixed and is calculated from the average of the four curves at higher exposure (the curves that reach the plateau at F_a = 1 allow for more accurate fits). Fig. 3b shows that the higher OH exposure and the more $\mu_{\kappa,\text{geo}}$ shifts to higher values (the particles become more hygroscopic). As the trends for kerosene and diesel soot particles are similar, only kerosene soot is shown in the figure.

4.2.2 Comparison between kerosene and diesel soot

From the previous analysis, a comparison of the hygroscopic properties of kerosene and diesel soot is shown in Fig. 4 using the median value of the p(κ) distribution (see Fig. 3b) and SS_c. Data are plotted as function of d_{ve} and the range of investigated OH exposures is represented by a color chart. Kerosene and diesel soot particles sampled at HAB=130 mm behave very similarly. At constant OH exposure, κ obtained in a premixed ethylene flame [10] is much smaller, confirming the strong dependence of κ with the type of soot particles [11]. SS_c decreases with the increase of OH exposure.

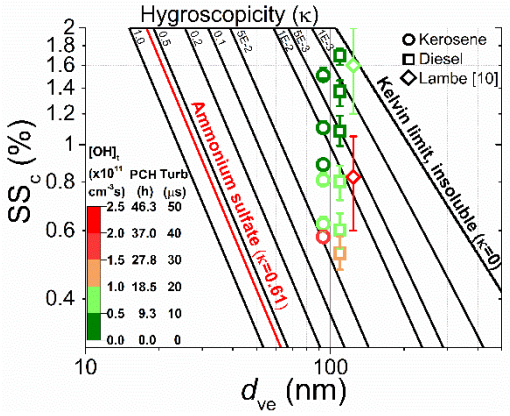

Figure 4: SS_c against d_{ve}. Kerosene soot, diesel soot and ethylene soot from reference [10] are presented by rounds, squares and diamonds, respectively. OH exposure is presented by the color map (green to red). Also represented the atmospheric photochemical age in hours (PCH) and the residence time in the turbine (Turb) as explained below. A high quality version of Fig.4 is provided in SM5.

Globally, the behavior of both types of soot particles after chemical aging is very similar, indicating that under our experimental conditions: (1) fresh soot is not active regardless of the fuel, (2) sulfur contained in the fuel up to 700 ppm does not promote the affinity of soot particles exposed to OH to form CCNs, and (3) the higher OH exposure, the larger κ which reaches 0.05. In our experiments,

sulfur gaseous compounds and volatile organic compounds have been deliberately removed by the denuder to prevent secondary organic aerosol formation in the simulation chamber. The presence of these potentially strong hydrophilic agents, if partially condensed onto soot surface, may increase soot activity.

The above results can be interpreted in two different ways:

In terms of atmospheric impact. When kerosene soot is exposed to OH radicals in the atmospheric simulation chamber, SS_c ranges between 0.5 and 0.8 % for OH exposure between 1.9 10^{11} and 5 10^{10} molecule cm^{-3} s. This range of SS_c is consistent with tropospheric conditions during cloud formation process [28]. The concentration of OH in the troposphere varies considerably depending on the time of day (very low during the night and up to 6-8 × 10^6 molecule.cm^{-3} at noon), altitude and geographic area [29]. Using a mean concentration [OH]= 1.5 × 10^6 molecule.cm^{-3} as measured at high altitude by aircraft measurements [30], and considering the above range of OH exposures , a soot particle would need between around 9 and 28 hours to be activated in the troposphere (see chart of photochemical age in Fig. 4). Since the global mean atmospheric lifetime of soot is estimated to be around 4 days [31], CCN activation of soot by OH oxidation is an atmospheric aging process which should be taken into account.

- In terms of impact on contrail formation. At present, the first steps of contrails formation in the models is mostly driven by the immersion or contact freezing of liquid H_2SO_4/H_2O droplets already nucleated from soot CCN [5-6]. H_2SO_4 concentration is calculated in [32] by modeling the evolution of the chemical composition of the exhausts upstream the turbine exit. Our results indicate that exposition to OH can make the soot hydrophilic. Concerning OH concentration in the vicinity of aeronautic turbines, mole fractions as low as 1-100 ppb are measured in exhaust by laser-induced fluorescence [32,33]. By contrast, OH is known to exist in much larger concentration in flames and postflames as long as the temperature is high enough.

Admittedly, our experiment set-up is not a contrail generator. It is performed under ambient conditions and uses kerosene (or diesel) soot produced in atmospheric jet flames, which is then

oxidized in the simulation chamber. But we got evidence that OH aging greatly promotes the hygroscopicity of soot particles. The possibility that soot exiting the turbine may have been sufficiently oxidized to become CCN has never been explored although the possible role of OH was evocated in [15]. In aircraft engines, combustion and soot production occur in the primary zone of the chamber, followed by a secondary zone where the burnt gases are highly diluted and cooled with fresh air. In this post-flame zone, soot particles are largely oxidized by the excess air. This might explain why the diameter of primary soot particles emitted by commercial aircraft engines is found relatively small around 15-16 nm on a large range of engine thrusts [34,35] by contrast to the much larger diameter of soot particles sampled in the sooting zone of high pressure combustors [36]. In the next section, we evaluate whether the exposure of soot particles to OH radicals, present between the combustor and the exit of an aeronautic engine, could be high enough to make them sufficiently active to become CCNs.

5. Computational fluid dynamics simulation

To verify the true OH exposure of soot in real engine conditions, results from CFD simulations are analyzed in a post-processing step. In an aeronautical turbofan engine, the combustion chamber exits in high pressure (HP) turbine through which the flow experiences strong deviation and acceleration as well as cooling and to a lesser extent pressure drop, during a residence time of the order of 1 ms (Fig. 5a). The HP turbine gives rotation to the flow, in same direction of the rotating low pressure (LP) turbine placed downstream and allowing to expand the flow to the atmosphere while extracting work. The HP turbine is usually made of one stator stage, with cooled blades as illustrated in Fig. 5b. To estimate the evolution of the burnt gases in the HP turbine, a series of fluid particle trajectories is extracted from a previously computed Large Eddy Simulation (LES) of a representative configuration with the code AVBP of CERFACS [37]. The LES is performed for a compressible non reacting air flow, and allows obtaining the unsteady 3D velocity, pressure and temperature solution fields. Fluid particle trajectories are obtained by randomly seeding the flow at

the inlet of the HP turbine (red arrow in Fig. 5b). Examples of time evolutions of pressure and temperature recorded along the trajectories are shown in SM6. These evolutions p(t) and T(t) are then imposed to unsteady 0D chemical reactor calculations, performed with the code CANTERA [38]. Starting from initial conditions corresponding to burnt gas equilibrium at p_0 and T_0 conditions at the chamber exit (i.e. HP turbine inlet), the time evolution of the mixture composition is calculated with the detailed chemical kinetics of [39] for dodecane, a simple kerosene surrogate which allows correct prediction of major species in the burnt gases. In small power aeronautical combustion chamber, HP inlet conditions are typically p_0=7.5 × 10^3 mbar and T_0=1750 K, and the pressure may increase to 20 × 10^3 mbar in higher thrust engines for civil aviation. Calculations have shown that the OH mass fraction increases with pressure so that the less favorable case, with low p_0 is considered here. A typical evolution of OH is shown in SM6. From these input conditions the mean OH mass fraction in the HP turbine is calculated around 9.7×10^{-5}, which converts into an OH concentration of 5×10^{15} molecule cm^{-3}. Incorporating this value in the color chart of Fig. 4, and assuming that κ values extracted from our experiments at ambient conditions can be transferred to the turbine conditions, shows that only 0.05 ms in the HP turbine is required to achieve the same OH exposure as the highest one reached in CESAM chamber. The residence time computed as the average duration of particle trajectories in the HP turbine being around 0.6 ms [SM6], this calculation indicates that soot particles can be activated just from their OH oxidation within the turbine, opening a new possible route to be considered for understanding the formation of first ice particles.

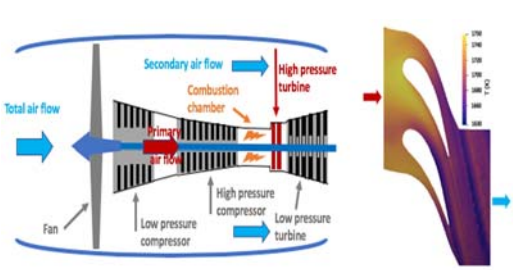

Figure 5: (a:left) Sketch of an aeronautical engine. The part in red downstream the combustion chamber is the high pressure turbine, through which the evolution of OH concentration has been calculated. (b:right) Temperature (K) field in the HP turbine.

6. Conclusion

In this work, the hygroscopic properties of soot formed in a turbulent jet flame supplied with kerosene or diesel are studied in water supersaturation conditions and ambient temperature. These fresh soot particles being hydrophobic, oxidation with OH radicals is chosen to promote activation using the CESAM simulation chamber. The activated fraction is measured for size-selected soot particles against OH exposures using a cloud condensation nuclei counter. The role of the fuel sulfur content in enhancing soot activation is also investigated. The hygroscopic parameter κ is determined using a model based on extended κ-Köhler theory. Results show that diesel and kerosene particles behave very similarly with κ reaching 0.05 for OH exposure of 1.9×10^{11} molecule cm^{-3} s.

To assess whether the oxidation of soot particles by OH radicals formed in aeronautical engines during their transport in the turbine is sufficient to promote activation, the large eddy simulation in the high pressure turbine is used to model the fluid particle trajectories and their chemical evolution by means of a detailed chemical mechanism and the input equilibrium composition of the burnt gases. The calculated mean OH concentration is 5×10^{15} molecule cm^{-3}. From the chart in Fig.4, representing SS_c as function of d_{ve} for different OH exposures, one deduces that 0.05 ms only, i.e. one tenth of the typical residence time of soot in the turbine, is sufficient to achieve κ=0.05, thus converting soot particles into potential CCNs. This estimation implicitly assumes that the activity of soot is similar at ambient conditions or in the turbine. It is probable that it is even more important at high temperature. In addition calculations performed with higher inlet pressure (for higher thrusts) lead to a much higher OH mass fraction. Even though our nucleation chamber works in water supersaturation at ambient conditions i.e. far from the tropospheric ones, it must be noticed that the temperature range encountered in the early turbine wakes is 280-440 K [40]. Therefore we are

confident that the main conclusion of our work, i.e. that OH oxidation in the turbine is a potentially important activation agent of soot, is at least qualitatively, transposable to the early steps of contrail formation, opening a new possible route to be considered for understanding the formation of first ice particles. Presence of OH radicals in the burnt gases being unavoidable, mitigation of contrails requires a reduction of the soot emission index. In addition this study also shows that sulfur contained in the fuel up to 700 ppm does not affect soot particle hygroscopicity and therefore has a weak impact on the contrail formation.

Acknowledgements:

This work was supported by the MERMOSE project sponsored by DGAC (French Civil Aviation Authority), the Labex CaPPA under contract ANR-11-LABX-0005-01 and by the CPER CLIMIBIO, the Région Hauts-de-France and the European Funds for Regional Economical Development. CNRS-INSU is gratefully acknowledged for supporting the CESAM chamber as a national facility. We thank B. Martin et L. Gicquel (CERFACS) for their contribution in CFD calculations and Claudia Di Biagio for assistance with chamber experiments.

SMM.pdf file

References

[1] B. Kärcher, Formation and radiative forcing of contrail cirrus, Nat. Commun. 9 (2018) 1824. https://doi.org/10.1038/s41467-018-04068-0.

[2] U. Schumann, R. Baumann, D. Baumgardner, S.T. Bedka, D.P. Duda, V. Freudenthaler, J.-F. Gayet, A.J. Heymsfield, P. Minnis, M. Quante, E. Raschke, H. Schlager, M. Vázquez-Navarro, C. Voigt, Z. Wang, Properties of individual contrails: a compilation of observations and some comparisons, Atmos. Chem. Phys. 17 (2017) 403–438. https://doi.org/10.5194/acp-17-403-2017.

[3] H. Appleman, The formation of exhaust condensation trails by jet aircraft, Bull. Amer. Meteor. Soc. 34 (1953) 14–20.

[4] U. Schumann, A contrail cirrus prediction model, Geosci. Model Dev. 5 (2012) 543–580. https://doi.org/10.5194/gmd-5-543-2012.

[5] H.-W. Wong, P.E. Yelvington, M.T. Timko, T.B. Onasch, R.C. Miake-Lye, J. Zhang, I.A. Waitz, Microphysical modeling of ground-level aircraft-emitted aerosol formation: roles of sulfur-containing species, J. Propul. Power. 24 (2008) 590–602. https://doi.org/10.2514/1.32293.

[6] R. Paoli, K. Shariff, Contrail modeling and simulation, Annu. Rev. Fluid Mech. 48 (2016) 393–427. https://doi.org/10.1146/annurev-fluid-010814-013619.

[7] J.C. Khou, W. Ghedhaïfi, X. Vancassel, E. Montreuil, F. Garnier, CFD simulation of contrail formation in the near field of a commercial aircraft: effect of fuel sulfur content, Meteorol. Z. 26 (2017) 585–596. https://doi.org/10.1127/metz/2016/0761.

[8] B. Kärcher, F. Yu, Role of aircraft soot emissions in contrail formation, Geophys. Res. Lett. 36 (2009) L01804. https://doi.org/10.1029/2008GL036649.

[9] C. Wittbom, A.C. Eriksson, J. Rissler, J.E. Carlsson, P. Roldin, E.Z. Nordin, P.T. Nilsson, E. Swietlicki, J.H. Pagels, B. Svenningsson, Cloud droplet activity changes of soot aerosol upon smog chamber ageing, Atmos. Chem. Phys. 14 (2014) 9831–9854. https://doi.org/10.5194/acp-14-9831-2014.

[10] A.T. Lambe, A.T. Ahern, J.P. Wright, D.R. Croasdale, P. Davidovits, T.B. Onasch, Oxidative aging and cloud condensation nuclei activation of laboratory combustion soot, J. Aerosol Sci. 79 (2015) 31–39. https://doi.org/10.1016/j.jaerosci.2014.10.001.

[11] S. Grimonprez, A. Faccinetto, S. Batut, J. Wu, P. Desgroux, D. Petitprez, Cloud condensation nuclei from the activation with ozone of soot particles sampled from a kerosene diffusion flame, Aerosol Sci. Technol. 52 (2018) 814–827. https://doi.org/10.1080/02786826.2018.1472367.

[12] B. Zuberi, K.S. Johnson, G.K. Aleks, L.T. Molina, M.J. Molina, A. Laskin, Hydrophilic properties of aged soot, Geophys. Res. Lett. 32 (2005) L01807. https://doi.org/10.1029/2004GL021496.

[13] A. Petzold, M. Gysel, X. Vancassel, R. Hitzenberger, H. Puxbaum, S. Vrochticky, E. Weingartner, U. Baltensperger, P. Mirabel, On the effects of organic matter and sulphur-containing compounds on the CCN activation of combustion particles, Atmos. Chem. Phys. 5 (2005) 3187–3203. https://doi.org/10.5194/acp-5-3187-2005.

[14] J. Wang, J.F. Doussin, S. Perrier, E. Perraudin, Y. Katrib, E. Pangui, B. Picquet-Varrault, Design of a new multi-phase experimental simulation chamber for atmospheric photosmog, aerosol and cloud chemistry research, Atmos. Meas. Tech. 4 (2011) 2465–2494. https://doi.org/10.5194/amt-4-2465-2011.

[15] B. Kärcher, T. Peter, U.M. Biermann, U. Schumann, The initial composition of jet condensation trails, J. Atmos. Sci. 53 (1996) 3066–3083. https://doi.org/10.1175/1520-0469(1996)053<3066:TICOJC>2.0.CO;2.

[16] M.D. Petters, S.M. Kreidenweis, A single parameter representation of hygroscopic growth and cloud condensation nucleus activity, Atmos. Chem. Phys. 7 (2007) 1961–1971. https://doi.org/10.5194/acp-7-1961-2007.

[17] J. Wu, A. Faccinetto, S. Grimonprez, S. Batut, J. Yon, P. Desgroux, D. Petitprez, Influence of the dry aerosol particle size distribution and morphology on the cloud condensation nuclei

activation. An experimental and theoretical investigation, Atmos. Chem. Phys. 20 (2020) 4209–4225. https://doi.org/10.5194/acp-20-4209-2020.
[18] P. Parent, C. Laffon, I. Marhaba, D. Ferry, T.Z. Regier, I.-K. Ortega, B. Chazallon, Y. Carpentier, C. Focsa, Nanoscale characterization of aircraft soot: a high-resolution transmission electron microscopy, Raman spectroscopy, X-ray photoelectron and near-edge X-ray absorption spectroscopy study, Carbon. 101 (2016) 86–100. https://doi.org/10.1016/j.carbon.2016.01.040.
[19] R. Lemaire, E. Therssen, P. Desgroux, Effect of ethanol addition in gasoline and gasoline–surrogate on soot formation in turbulent spray flames, Fuel. 89 (2010) 3952–3959. https://doi.org/10.1016/j.fuel.2010.06.031.
[20] J. Yon, R. Lemaire, E. Therssen, P. Desgroux, A. Coppalle, K.F. Ren, Examination of wavelength dependent soot optical properties of diesel and diesel/rapeseed methyl ester mixture by extinction spectra analysis and LII measurements, Appl. Phys. B. 104 (2011) 253–271. https://doi.org/10.1007/s00340-011-4416-4.
[21] J.F. Pauwels, M. Carlier, P. Devolder, L.R. Sochet, The influence of hydrogen sulfide on the combustion of methanol in a stoichiometric premixed flame. experimental and numerical studies, Combust. Sci. Technol. 86 (1992) 237–252. https://doi.org/10.1080/00102209208947197.
[22] T. Tritscher, Z. Jurányi, M. Martin, R. Chirico, M. Gysel, M.F. Heringa, P.F. DeCarlo, B. Sierau, A.S.H. Prévôt, E. Weingartner, U. Baltensperger, Changes of hygroscopicity and morphology during ageing of diesel soot, Environ. Res. Lett. 6 (2011) 034026.
[23] P. Barmet, J. Dommen, P.F. DeCarlo, T. Tritscher, A.P. Praplan, S.M. Platt, A.S.H. Prévôt, N.M. Donahue, U. Baltensperger, OH clock determination by proton transfer reaction mass spectrometry at an environmental chamber, Atmos. Meas. Tech. 5 (2012) 647–656. https://doi.org/10.5194/amt-5-647-2012.
[24] M. Lendar, A. Aissat, M. Cazaunau, V. Daële, A. Mellouki, Absolute and relative rate constants for the reactions of OH and Cl with pentanols, Chem. Phys. Lett. 582 (2013) 38–43. https://doi.org/10.1016/j.cplett.2013.07.042.
[25] H. Abdul-Razzak, S.J. Ghan, A parameterization of aerosol activation: 2. Multiple aerosol types, J. Geophys. Res. Atmos. 105 (2000) 6837–6844. https://doi.org/10.1029/1999JD901161.
[26] H. Su, D. Rose, Y.F. Cheng, S.S. Gunthe, A. Massling, M. Stock, A. Wiedensohler, M.O. Andreae, U. Pöschl, Hygroscopicity distribution concept for measurement data analysis and modeling of aerosol particle mixing state with regard to hygroscopic growth and CCN activation, Atmos. Chem. Phys. 10 (2010) 7489–7503. https://doi.org/10.5194/acp-10-7489-2010.
[27] J. Yon, A. Bescond, F.-X. Ouf, A simple semi-empirical model for effective density measurements of fractal aggregates, J. Aerosol Sci. 87 (2015) 28–37. https://doi.org/10.1016/j.jaerosci.2015.05.003.
[28] H.R. Pruppacher, J.D. Klett, Microphysics of Clouds and Precipitation, 2nd ed., Springer Netherlands, 2010. https://www.springer.com/fr/book/9780792342113.
[29] D. Stone, L.K. Whalley, D.E. Heard, Tropospheric OH and HO2 radicals: field measurements and model comparisons, Chem. Soc. Rev. 41 (2012) 6348–6404. https://doi.org/10.1039/C2CS35140D.
[30] J. Mao, X. Ren, W.H. Brune, J.R. Olson, J.H. Crawford, A. Fried, L.G. Huey, R.C. Cohen, B. Heikes, H.B. Singh, D.R. Blake, G.W. Sachse, G.S. Diskin, S.R. Hall, R.E. Shetter, Airborne measurement of OH reactivity during INTEX-B, Atmos. Chem. Phys. 9 (2009) 163–173. https://doi.org/10.5194/acp-9-163-2009.
[31] X. Wang, C.L. Heald, D.A. Ridley, J.P. Schwarz, J.R. Spackman, A.E. Perring, H. Coe, D. Liu, A.D. Clarke, Exploiting simultaneous observational constraints on mass and absorption to estimate the global direct radiative forcing of black carbon and brown carbon, Atmos. Chem. Phys. 14 (2014) 10989–11010. https://doi.org/10.5194/acp-14-10989-2014.
[32] C.W. Wilson, A. Petzold, S. Nyeki, U. Schumann, R. Zellner, Measurement and prediction of emissions of aerosols and gaseous precursors from gas turbine engines (PartEmis): an overview, Aerosp. Sci. Technol. 8 (2004) 131–143. https://doi.org/10.1016/j.ast.2003.10.006.

[33] S. Böckle, S. Einecke, F. Hildenbrand, C. Orlemann, C. Schulz, J. Wolfrum, V. Sick, Laser-spectroscopic investigation of OH-radical concentrations in the exhaust plane of jet engines, Geophys. Res. Lett. 26 (1999) 1849–1852. https://doi.org/10.1029/1999GL900364.
[34] D. Delhaye, F.-X. Ouf, D. Ferry, I.-K. Ortega, O. Penanhoat, S. Peillon, F. Salm, X. Vancassel, C. Focsa, C. Irimiea, N. Harivel, B. Perez, E. Quinton, J. Yon, D. Gaffie, The MERMOSE project: characterization of particulate matter emissions of a commercial aircraft engine, J. Aerosol Sci. 105 (2017) 48–63. https://doi.org/10.1016/j.jaerosci.2016.11.018.
[35] A. Liati, B.T. Brem, L. Durdina, M. Vögtli, Y. Arroyo Rojas Dasilva, P. Dimopoulos Eggenschwiler, J. Wang, Electron microscopic study of soot particulate matter emissions from aircraft turbine engines, Environ. Sci. Technol. 48 (2014) 10975–10983. https://doi.org/10.1021/es501809b.
[36] B. Gigone, A.E. Karataş, Ö.L. Gülder, Soot aggregate morphology in coflow laminar ethylene diffusion flames at elevated pressures, Proc. Combust. Inst. 37 (2019) 841–848. https://doi.org/10.1016/j.proci.2018.06.103.
[37] B. Martin, M. Thomas, J. Dombard, F. Duchaine, L.Y.M. Gicquel, Analysis of solid particle ingestion and dynamics in a turbomachine using large eddy simulation, in: Proceedings of the ASME 2019 Turbo Expo, The American Society of Mechanical Engineers (ASME), Phoenix, USA, 2019: pp. 1–13.
[38] D.G. Goodwin, R.L. Speth, H.K. Moffat, B.W. Weber, CANTERA: an object-oriented software toolkit for chemical kinetics, thermodynamics, and transport processes, 2019. https://doi.org/10.5281/zenodo.1174508.
[39] H. Wang, E. Dames, B. Sirjean, D.A. Sheen, R. Tango, A. Violi, J.Y.W. Lai, F.N. Egolfopoulos, D.F. Davidson, R.K. Hanson, C.T. Bowman, C.K. Law, W. Tsang, N.P. Cernansky, D.L. Miller, R.P. Lindstedt, JetSurF version 2.0. A high-temperature chemical kinetic model of n-alkane (up to n-dodecane), cyclohexane, and methyl-, ethyl-, n-propyl and n-butyl-cyclohexane oxidation at high temperatures, 2010. http://web.stanford.edu/group/haiwanglab/JetSurF/JetSurF2.0/index.html.
[40] R. Paoli, J. Hélie, T. Poinsot, Contrail formation in aircraft wakes, J. Fluid Mech. 502 (2004) 361–373. https://doi.org/10.1017/S0022112003007808.

Figure and table captions

Figure 1: Schematic of the experimental setup

Figure 2: d_m of kerosene soot versus aging time in CESAM. Concentration is represented by white-blue heat map. Solid red squares represent the median of the size distribution. t=0 refers to the OH generation.

Fig 3: (a) Activated fraction F_a versus water supersaturation SS_w: activation curves of kerosene soot particles exposed to OH radicals. Experimental data (solid points) are fitted using the extended κ-Köhler model [17]. (b) probability density function p(κ) versus hygroscopicity parameter κ: log normal distribution of κ of kerosene soot particles exposed to OH radical.

Figure 4: SS_c against d_{ve}. Kerosene soot, diesel soot and ethylene soot from reference [10] are presented by rounds, squares and diamonds, respectively. OH exposure is presented by the color map (green to red). Also represented the photochemical age in hours (PCH) and the residence time in the turbine (Turb) as explained below. A high quality version of Fig.4 is provided in SM5.

Figure 5: (left) Sketch of an aeronautical engine. The part in red downstream the combustion chamber is the high pressure turbine, through which the evolution of OH concentration has been calculated. (right) Temperature (K) field in the HP turbine.

Table 1: Table 1: Morphological parameters of soot particles selected and sent to the CCNc with d_m = 150 nm: primary particle diameter ($d_{pp,}$ nm), fractal dimension D_f, geometric mean $\mu_{p,geo}$ and standard deviation $\sigma_{p,geo}$ of d_m distribution (nm). d_{pp} and D_f are determined from TEM analysis [11,20].